

An attempt to locate substorm onsets using Pi1 signatures

V.A. Pilipenko, I.I. Tchebotareva, M.J. Engebretson, J.L. Posch, and A. Rodger

Abstract: Pi1 observations, because of their higher frequency, hold the promise of providing better temporal resolution for accurate timing of substorm onsets, thus continuing to be a matter of considerable importance for evaluation of competing substorm mechanisms. In this presentation we show that the same Pi1 signatures detected by the ground magnetometer array can be used also for the spatial location of substorm onsets. We have used data from Antarctic search-coil magnetometers. To locate an ionospheric source of Pi1 signatures we have applied a method of emission tomography that was previously used in seismology. The source image reconstruction algorithm uses scanning of the volume under investigation; for each of the grid points a coherency measure for multi-channel data is calculated. For the source image reconstruction we have introduced a coherency measure, that may be coined the nonlinear semblance. Though the Antarctic stations are elongated in one direction, that is not favorable for tomography methods, the results obtained seems to be very promising for locating substorm onsets with ground magnetometer data.

Key words: substorm onset, ULF pulsations, auroral activation, tomography.

1. Introduction

Accurate timing and locating of substorm onsets continues to be a matter of considerable importance as the space physics community tries to evaluate competing onset mechanisms. Although UV satellite imagers provide onset location of unparalleled quality, the paucity of satellites and their limited imaging cadence underscore the need for complementary, ground-based monitoring techniques. The long-period nature of Pi2 signals provides only approximate timing (\sim few min). A spatial pattern of Pi2 signatures in the auroral region is rather complicated, which hampers a straightforward backward ray tracing. Pi1 observations, because of their higher frequency, hold the promise of providing better temporal resolution (\sim few sec) [1]. In contrast to longer-period Pi2 signals, part of Pi1 wave burst can be trapped in the ionospheric waveguide and propagate along the ionosphere nearly isotropically.

2. Current understanding of Pc1/Pi1 signal propagation from an ionospheric source

The ULF waves in the Pc1/Pi1 band are expected to be produced through field-aligned injection of the localized Alfvén wave into the ionosphere. MHD waves in the frequency range around 1 Hz are regarded to propagate in the horizontal direction after being trapped in the upper ionosphere. Thus, a horizontal profile of Pc1/Pi1 magnetic signals is determined by both the mode conversion from incident Alfvén waves into horizontally propagating fast magnetosonic waves owing to anisotropic Hall conductance and trapping of the fast wave in the ionospheric F-layer [4]. The spatial and frequency dependences of the ground magnetic signal are to be different in two

separate regions: in the injection center and in a region with distance much larger than the scale of the incident wave. In the center ($r < r_0$, where r_0 is the scale of localization of the incident wave), ground magnetic field disturbances have the same spatial properties of intensity and polarization as those of an incident Alfvén wave. In the far-off region ($r \gg D$, where D is the scale of the waveguide), the electromagnetic field of the fast wave is dominant. In the intermediate transition region between those two regions a numerical approach is necessary to describe the wave pattern.

In a two-layer model (1-magnetosphere, 2 - ducting F-layer), a fast wave with $k_n V_A^{(2)} < \omega < k_n V_A^{(1)}$ is trapped: it is vertically evanescent in the magnetosphere and simultaneously is propagating along the ducting layer. The horizontal wave number k_n increases in association with an increase of frequency: at the lower cutoff it is $\omega/V_A^{(1)}$ and tends to be $\omega/V_A^{(2)}$ in the higher frequency limit. Both phase and group velocities tend to $V_A^{(1)}$ at the lower cutoff frequency and to $V_A^{(2)}$ at higher frequency. Each harmonic wave has a minimum group velocity less than the ionospheric Alfvén velocity $V_A^{(2)}$. However, the effective average damping rate and apparent propagation velocity are expected to be substantially lower, because in the central and intermediate regions the signal is dominated by Alfvén waves and horizontal propagation does not play a significant role. The important results of analytical and numerical models of MHD wave excitation and propagation in the ionosphere [3] are summarized as follows:

The observed damping rate is about 10dB/100km as a maximum in the injection region and about 2.5dB/100km in the region beyond 500 km. Spatial attenuation is larger in the daytime than in the nighttime;

The ducted wave has a lower cutoff frequency. Attenuation of the ducted wave is generally minimized at the lower cutoff frequency. The attenuation of ducted waves propagating off the geomagnetic meridian is larger than in the meridian plane.

It would be fair to say that we are not aware of any observational study that has unambiguously shown that Pi1 propagation along the Earth's surface is due to ionospheric waveguide

Received 7 June 2006.

V.A. Pilipenko and I.I. Tchebotareva. Institute of the Physics of the Earth, Moscow
M.J. Engebretson and J.L. Posch. Augsburg College, MN
A. Rodger. British Antarctic Survey, Cambridge, UK

propagation. However, the approach used here does not in fact depend on the actual propagation mode, but just assumes isotropic horizontal propagation from a source with some averaged velocity.

3. Observational data

We analyze Pi 1 signatures detected by an array of Antarctic search-coil magnetometers. The locations of these stations are shown in Figure 1. Pi1 were observed predominantly when the ground stations were near local midnight (within several hours of MLT). The coordinates and codes of Antarctic stations can be found elsewhere.

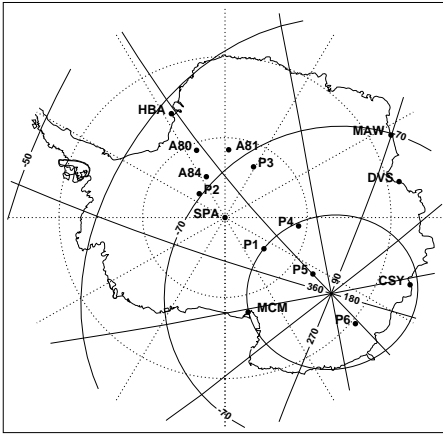


Fig. 1. Map of search-coil magnetometers in Antarctica. Solid lines denote geomagnetic coordinates, and dotted lines denote geographic coordinates.

4. Algorithm of the source location

To locate an ionospheric source of Pi 1 signatures we have applied the method of emission tomography that was previously used in seismology [5]. This method does not require a picking of onset arrival time in contrast to many other methods of a signal source location. Therefore, it makes it possible to locate simultaneously a few interference events, events with illegible onsets, and events with very weak signals that are nearly obscured by noise. The method permits the processing of both one component data and three component data with polarization focusing. In seismology, emission tomography can provide three-dimensional seismic source distribution, i.e., estimation of their azimuths, apparent distances, and depths.

The idea of the method is as follows. Suppose that a small volume radiates a weak signal with a simple structure, e.g., a spherical wave in a homogeneous medium. In a realistic medium, the signal trajectory may be distorted due to velocity inhomogeneity, but a spatial signal coherence remains. This fact is used for source detection. The source image reconstruction algorithm uses scanning of the volume under investigation over the points of a grid. For each of the grid points a coherency measure for multi-channel data is calculated. One derives

the spatial distribution of the coherency measure that characterizes the emission properties of a medium by scanning the structure over a multi-dimensional rectangular grid.

For the source image reconstruction a different coherency measure may be used, traditionally the semblance S [7]. If there is no coherent component in recorded data and only independent evenly distributed Gaussian noise is present on each channel, the semblance has a β -distribution with expected mean and variance [5]. That is, when no signal is present, semblance maps provide a uniform distribution of brightness. When coherent signals from an emission source occur in the noise-like wave field, a bright spot appears in the reconstructed image. Semblance sharply increases for those grid points which are closer to the source. Semblance is a function of the signal-to-noise ratio and for a weak signal equals to the product of the signal to noise ratio and the number of channels.

The scale of the bright spot around the probable source location in the image is proportional to the dominant signal wave length. We had intended going to process signal with large wave length, but preliminary analyses of real data resulted in poor spatial resolution. That is why in this work we decided to use another coherent measure. Numerical simulation and analysis of real data has shown that the use of this new coherent measure greatly improves the quality of source images and results in a considerably better spatial resolution. The conventional semblance S is described by the formula

$$S = \frac{\sum_{j=1}^T \left(\sum_{i=1}^K f_{ij}(\tau_i) \right)^2}{\sum_{j=1}^T \sum_{i=1}^K f_{ij}^2(\tau_i)} \quad (1)$$

where f_{ij} is the instantaneous amplitude of the j -th sample at the i -th recording site, K is the number of channels, and T is the time window length in samples. The parameter τ_i is the time shift in the i -th channel appropriate to the path of a hypothetical signal from a focused grid point, and determined by the propagation with velocity V . In this version of the algorithm isotropic propagation is assumed, but it could be extended to the case of non-isotropic propagation. The term in parenthesis in the S numerator is coined linear or conventional beamforming. Instead, we use N -th root beamforming that is known to have a better directivity [6]. Our new measure, which may be coined a nonlinear semblance, is described by the formula

$$S = \frac{K^2 \sum_{j=1}^T B_j^2}{\sum_{j=1}^T \sum_{i=1}^K f_{ij}^2(\tau_i)} - 1 \quad (2)$$

where

$$B_j = |b_j|^N \quad b_j = \frac{1}{K} \sum_{i=1}^K |f_{ij}(\tau_i)|^{1/N} \text{sign}\{f_{ij}(\tau_i)\}$$

Here K , T , f_{ij} , and τ are the same parameters as for the conventional semblance (1), B_j is the N -th root beamforming, and N is the parameter of nonlinearity. Here we use $N = 4$ and one-component data. We have added -1 in the formula (2) because in this case in absence of signal the semblance is close to zero, $S \rightarrow 0$.

4.1. Pre-processing: The choice of frequency band and an apparent propagation velocity

Spectra of raw data show that Pi1 burst are broadband signals with spectral enhancement around 0.1 Hz (Figure 2). Therefore, raw search coil magnetometer data (H-component) have been preliminary band-pass filtered in the frequency band 0.05-0.3 Hz. The focusing process, that is the search of optimal

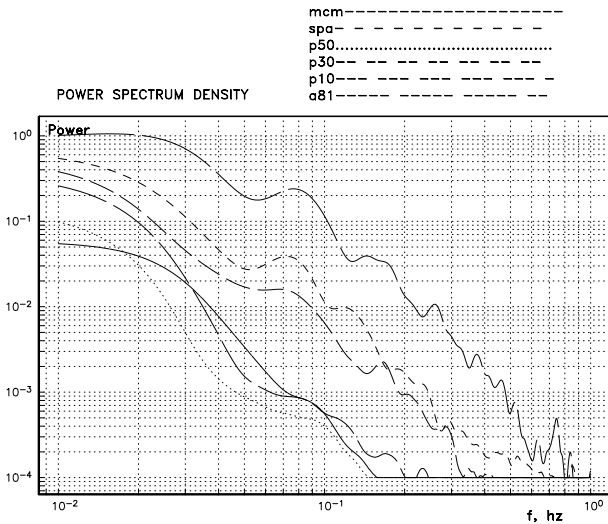


Fig. 2. Power spectral density of raw data from various Antarctic stations (indicated by different line patterns) for the event of January 03, 2001.

parameters for the brightest image of *S*, has been performed as follows. The start time is chosen in such a way to include the Pi1 burst onset from all stations into an interval to be analyzed. The length of the interval, or time window *T*, is to be larger than duration of signal burst.

The additional complications for the source location method is caused by the fact that the actual propagation velocity of a signal along the ionosphere is unknown. The idea of the optimal choice of an apparent average velocity is as follows. Test-and-try modeling provides the brightest (as characterized by the brightness rate *S*) and most focused image of a source when the selected apparent velocity of a signal matches the actual velocity.

5. Examples of the Pi1 source location with the nonlinear semblance algorithm

For each of the events below we show stacked line plots of raw search coil data with Pi1 signals. Two examples of Pi1 indicators of substorm onset will be analyzed and presented.

5.1. February 26, 2001 (day 057)

An intense Pi1 burst is evident at US (SPA, MCM) and British sites (A80, A81, A84) and Australian stations (MAW, DAV, CSY) around 0121 UT (Figure 3). The start time chosen is 0121 UT, and the time window is *T*=450s. The best-fit velocity was determined to be *V* =120 km/s.

The distribution of nonlinear semblance *S* constructed for this event is shown in Figure 4 as color-coded brightness. The

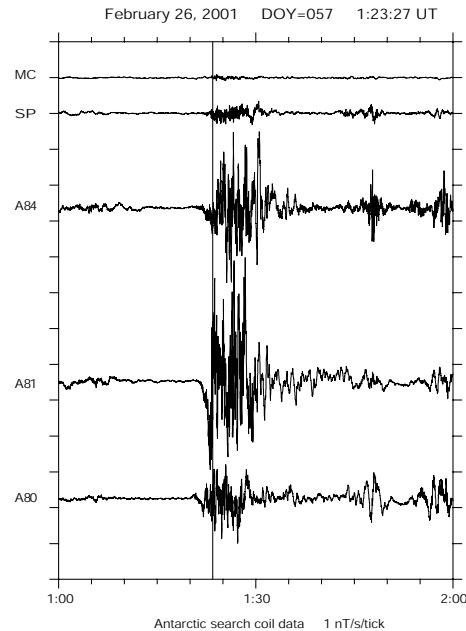


Fig. 3. The stacked raw magnetograms of Antarctic search-coil magnetometers for the event of February 26, 2001 (day 057).

semblance algorithm has found the epicenter of the Pi1 signal in an extended area equatorward from station A81.

5.2. January 3, 2001 (day 003)

A relatively weak substorm onset occurred at 0234 UT. Pi1 activity on raw records is evident at the two lowest latitude sites (A80, A81), and much weaker traces are at P3 and SPA (Figure 5), but on filtered records onset becomes evident at sites A80, A81, P1, P3, P5, SPA, and MCM. The start time is 0229 UT, and the time window is *T* =200 s. The best-fit velocity was determined to be *V* = 75 km/s. The Pi1 source location as determined by the algorithm is westward from SPA-P2 stations (Figure 6). This event shows that the algorithm is able to determine the source location even when a source is distant from the station array.

6. Conclusion

The location of available stations was very unfavorable for the emission tomography algorithm: practically all stations formed 1D array extended in North-South direction. However, even under these unfavorable conditions the nonlinear semblance algorithm has provided rather reasonable and consistent results. We suppose that this algorithm would be much more efficient for an actual 2D array. Hence, a dense spatial array of magnetometers sensitive to 0.1-1 Hz activity (both search coil instruments and low-noise fluxgate instruments) may provide both improved localization and timing information. The limited spatial range of Pi1 may prove to be an advantage in localizing onsets, and the range over which onsets stimulate Pi1 activity is limited in both local time and latitude.

It would be very interesting to compare the location of Pi1 source identified from ground-based magnetometers with UVI satellite images. Unfortunately, there were no satellite imager

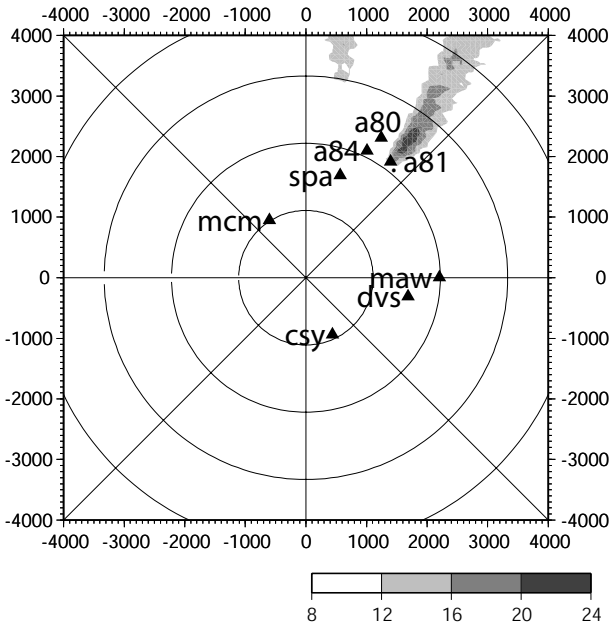


Fig. 4. Reconstruction of the Pi1 source location by the semblance method for the event February 26, 2001 (day 057).

observations over Antarctica during the period analyzed. Monitoring of Pi 1 activity can thus contribute to substorm studies in the absence of satellite imager data.

Acknowledgements. This study is supported by grant 03-51-5359 from INTAS (VAP, IIT, AR) and by National Science Foundation grant ATM-0305483 to Augsburg College (MJE, JLP). We acknowledge the data of Australian stations provided by P. Ponomarenko.

References

1. Bosinger, T., and A.G. Yahnin, Pi1B type magnetic pulsations as a high time resolution monitor of substorm development, *Ann. Geophysicae*, 5A, 231–238, 1987.
2. Douze, E.J., and S.J. Laster, Statistics of semblance, *Geophysics*, 44, 1999–2003, 1979.
3. Fujita S., and T. Tamao, Duct propagation of hydromagnetic waves in the upper ionosphere. 1. Electromagnetic field disturbances in high latitudes associated with localized incidence of a shear Alfvén wave, *J. Geophys. Res.*, 93, 14665–14673, 1988.
4. Greifinger, C., and P.S. Greifinger, Theory of hydromagnetic propagation in the ionospheric wave guide, *J. Geophys. Res.*, 73, 7473–7490, 1968.
5. Tchebotareva, I.I., A.V. Nikolaev, and H. Sato, Seismic emission activity of Earth’s crust in Northern Kanto, Japan, *Phys. Earth Planet. Interiors*, 120, 167–182, 2000.
6. Muirhead, K.J., and R. Datt, The N-th root process applied to seismic array data, *Geophys. J. R. Astr. Soc.*, 47, 197–210, 1976.
7. Taner, F., and N.S. Neidell, Semblance and other coherency measures for multichannel data, *Geophysica*, 36, 482–497, 1971.

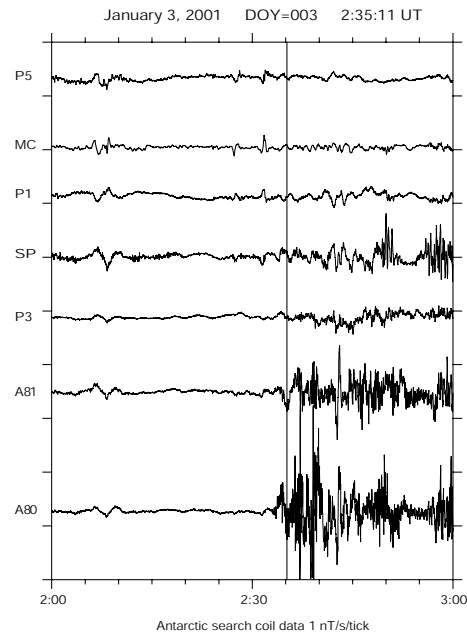


Fig. 5. The raw magnetograms of Antarctic search-coil magnetometers for the event of January 03, 2001 (day 003).

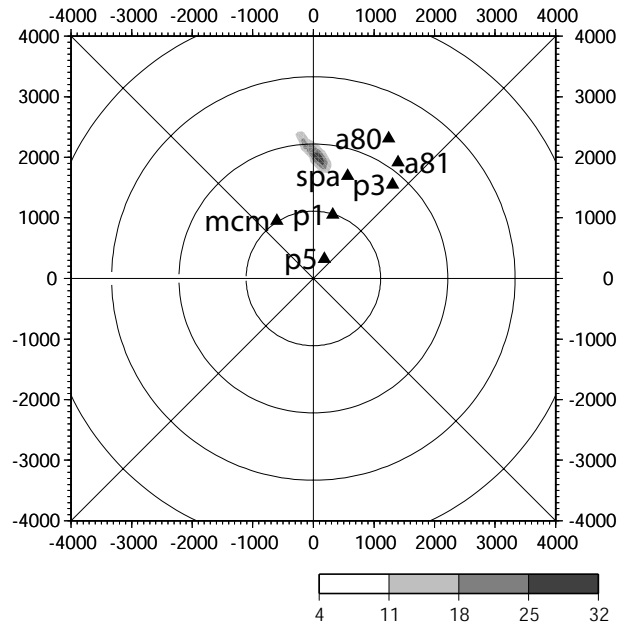


Fig. 6. Reconstruction of the Pi1 source location by the semblance method for the event of January 3, 2001 (day 003).